C. T.-C. Nguyen, "Transceiver front-end architectures using vibrating micromechanical signal processors (invited)," *Dig. of Papers*, Topical Meeting on Silicon Monolithic Integrated Circuits in RF Systems, Sept. 12-14, 2001, pp. 23-32.

Transceiver Front-End Architectures Using Vibrating Micromechanical Signal Processors

Clark T.-C. Nguyen

Center for Wireless Integrated Microsystems
Department of Electrical Engineering and Computer Science
University of Michigan
Ann Arbor, Michigan 48109-2122

Abstract

Transceiver architectures are proposed that best harness the tiny size, zero dc power dissipation, and ultra-high-*Q* of vibrating micromechanical resonator circuits. Among the more aggressive architectures proposed are one based on a micromechanical RF channel-selector and one featuring an all-MEMS RF front-end. These architectures maximize performance gains by using highly selective, low-loss micromechanical circuits on a massive scale, taking full advantage of *Q* versus power trade-offs. Micromechanical filters, mixer-filters, and switchable synthesizers are identified as key blocks capable of substantial power savings when used in the aforementioned architectures. As a result of this architectural exercise, more focused directions for further research and development in RF MEMS are identified.

I. Introduction

Recent demonstrations of vibrating beam micromechanical ("μmechanical") resonator devices with frequencies in the VHF range and *Q*'s in the tens of thousands (c.f., Fig. 1 [1]) have sparked a resurgence of research interest in communication architectures using high-*Q* passive devices. Much of the interest in these devices derives from their use of IC-compatible microelectromechanical systems (MEMS) fabrication technologies [2,3] to greatly facilitate the on-chip integration of ultra-high-*Q* passive tanks together with active transistor electronics, allowing substantial size reduction.

Although size reduction is certainly an advantage of this technology (commonly dubbed "RF MEMS"), it merely touches upon a much greater potential to influence general methods for signal processing. In particular, since they can now be integrated (perhaps on a massive scale) using MEMS technology, vibrating μmechanical resonators (or μmechanical links) can now be thought of as tiny circuit elements, much like resistors or transistors, in a new mechanical circuit technology. Like a single transistor, a single mechanical link does not possess adequate processing power for most applications. However, again like transistors, when combined into larger (potentially, VLSI) circuits, the true power of μmechanical links can be unleashed, and signal processing functions with attributes previously inaccessible to transistor circuits may become feasible. This in turn can lead to architectural changes for communication transceivers. MEMS technology may in fact make its most important impact not at the component level, but at the system level, by offering alternative transceiver architectures that emphasize selectivity to substantially reduce power consumption and enhance performance [4]. After reviewing the μmechanical devices most applicable to communications applications, this paper explores receiver and transmitter front-end architectures that can best harness the advantages of MEMS.

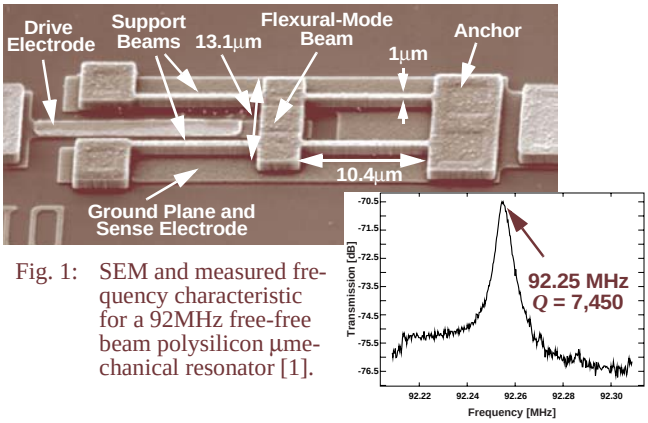

Fig. 1: SEM and measured frequency characteristic for a 92MHz free-free beam polysilicon μmechanical resonator [1].

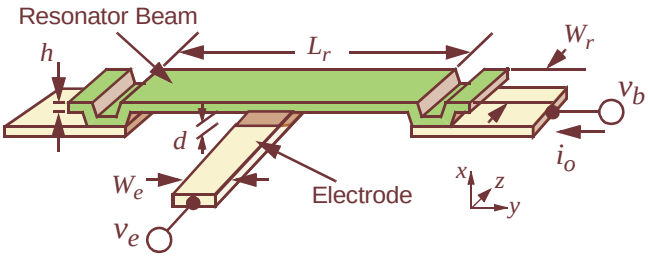

Fig. 2: Perspective-view schematic of a clamped-clamped beam μmechanical resonator in a general bias and excitation configuration.

II. Vibrating Micromechanical Signal Processors

For communications applications, clamped-clamped [5] and free-free [1] flexural-mode beams with *Q*'s on the order of 10,000 (in vacuum) and temperature coefficients on the order of −12ppm/^{o}C, have been popular for the VHF range, while thin-film bulk acoustic resonators [6] (*Q*~1,000) have so far addressed the UHF range. To simplify the discussion, and because they have so far been the most amenable to the implementation of mechanical circuits, this section will focus on clamped-clamped beam μmechanical resonators.

A. Clamped-Clamped Beam Micromechanical Resonators

Figure 2 presents the perspective-view schematic for a clamped-clamped beam μmechanical resonator, indicating key dimensions and showing a general bias and excitation configuration. As shown, this device consists of a beam anchored (i.e., clamped) at both ends, with an electrode underlying its central locations. Both the beam and electrode

Table I: μMechanical Resonator Frequency Design*

Freq. [MHz]	Material	Mode	h_r [μm]	W_r [μm]	L_r [μm]
70	silicon	1	2	8	14.54
110	silicon	1	2	8	11.26
250	silicon	1	2	4	6.74
870	silicon	2	2	4	4.38
870	diamond	2	2	4	8.88
1800	silicon	3	1	4	3.09
1800	diamond	3	1	4	6.16

* Determined for free-free beams using Timoshenko methods that include the effects of finite h and W_r [1].

are constructed of conductive materials, with doped polycrystalline silicon being the most common to date.

The vibrational resonance frequency f_o of the clamped-clamped beam of Fig. 2 is given approximately by the Euler-Bernoulli expression [5]

$$f_o = \frac{1}{2\pi}\sqrt{\frac{k_r}{m_r}} \cong 1.03\sqrt{\frac{E}{\rho}}\frac{h_{eff}}{L_r^2}(1-g(V_P))^{1/2}, \qquad (1)$$

where k_r and m_r are the effective stiffness and mass of the beam at a given location; E and ρ are the Young's modulus and density of the structural material, respectively; L_r is specified in Fig. 2; h_{eff} is an effective thickness that models the influence of surface topography on the beam in actual implementations, [5,7]; and the function g models the action of a dc-bias dependent electrical stiffness that adds to the mechanical stiffness of the beam, allowing some voltage-control of its frequency. From (1), geometry clearly plays a major role in setting the resonance frequency, and in practice, attaining a specified frequency amounts to CAD layout of the proper dimensions. In general, the resonance frequency of a mechanical resonator increases as its dimensions shrink (e.g., as the length of the beam in Fig. 2 decreases)—thus, the utility of micro- or nano-scale mechanical resonators for VHF to UHF communication applications. Table I presents expected resonance frequencies for free-free flexural-mode beams (c.f., Fig. 1) for various beam dimensions, modes, and structural materials, showing a wide range of attainable frequencies, from VHF to UHF. Although Table I was generated for free-free beams (which are more amenable to frequencies beyond VHF, c.f., Section II.C) using more accurate Timoshenko methods [1], the dimensions are nearly identical for clamped-clamped beams at the same frequencies.

As shown in Fig. 2, this device accepts two electrical inputs, v_e and v_b, applied to the electrode and beam, respectively. In this configuration, the difference voltage $(v_e - v_b)$ is effectively applied across the electrode-to-resonator capacitor gap, generating a force between the stationary electrode and the movable beam given by

$$F_d = \frac{\partial E}{\partial x} = \frac{1}{2}(v_e - v_b)^2\frac{\partial C}{\partial x} = \frac{1}{2}(v_e^2 - 2v_e v_b + v_b^2)\frac{\partial C}{\partial x} \qquad (2)$$

where x is displacement (with direction indicated in Fig. 2), and $(\partial C/\partial x)$ is the change in resonator-to-electrode capacitance per unit displacement. When using the resonator as a

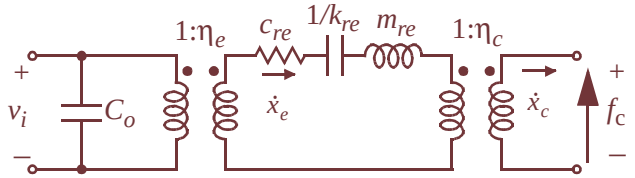

Fig. 3: Equivalent circuit for a mechanical beam element biased for tank or filter operation with one electrical port (voltage v_i) and one mechanical port (force f_c). Here, m_{re}, k_{re}, and c_{re} are the effective mass, stiffness, and damping factor at the location of the electrode center, and expressions for η_e and η_c are given in [5].

tank or filter circuit (as opposed to a mixer, to be discussed later), a dc-bias voltage V_P is applied to the conductive beam, while an ac excitation signal $v_i = V_i\cos\omega_i t$ is applied to the underlying electrode. In this configuration, (2) reduces to

$$F_d = \frac{\partial C}{\partial x}\left(\frac{V_P^2}{2} + \frac{V_i^2}{4}\right) - V_P\frac{\partial C}{\partial x}V_i\cos\omega_i t + \frac{\partial C}{\partial x}\frac{V_i^2}{4}\cos 2\omega_i t \qquad (3)$$

The first term in (3) represents an off-resonance dc force that statically bends the beam, but that otherwise has little effect on its signal processing function, especially for VHF and above frequencies. The second term constitutes a force at the frequency of the input signal, amplified by the dc-bias voltage V_P, and is the main input component used in tank and filter applications. When $\omega_i = \omega_o$ (the radian resonance frequency) this force drives the beam into resonance, creating a dc-biased (via V_P) time-varying capacitance between the electrode and resonator, and sourcing an output current $i_o = V_P(\partial C/\partial x)(\partial x/\partial t)$. When plotted versus the frequency of v_i, i_o traces out a bandpass biquad characteristic with a Q ~10,000 (c.f., Fig. 1)—very suitable for reference oscillators.

The third term in (3) represents a term capable of driving the beam into vibration when $\omega_i = (1/2)\omega_o$. If V_P is very large compared with V_i, this term is greatly suppressed, but can be troublesome for bandpass filters in cases where very large interferers are present at half the passband frequency. In these cases, a μmechanical notch filter at $(1/2)\omega_o$ may be needed.

In addition to electrical inputs, mechanical force inputs can also be applied at any location along the beam of Fig. 2, usually by connecting a forcing beam at the desired location. Accounting for both electrical and mechanical inputs, Fig. 3, presents the equivalent circuit for a beam element, such as depicted in Fig. 2, biased for tank or filter operation. Here, the electrode-to-resonator capacitor has been treated as a single electrical port, and a single mechanical port has also been added. In this circuit, a series LCR with element values proportional to the mass m_r, stiffness k_r, and damping c_r of the beam element, is used to model its high-Q bandpass characteristic. Transformers are then added to model the electrical-to-mechanical signal conversion occurring at the input electrode and the mechanical velocity transformation experienced when attaching a mechanical coupling beam at locations offset from the center of the beam [5].

In the design of μmechanical circuits comprised of interlinked beams, the equivalent circuit in Fig. 3 functions in a similar fashion to the hybrid-π small-signal equivalent circuit used for analog transistor circuit design. The main difference between mechanical links and transistors are the basic fea-

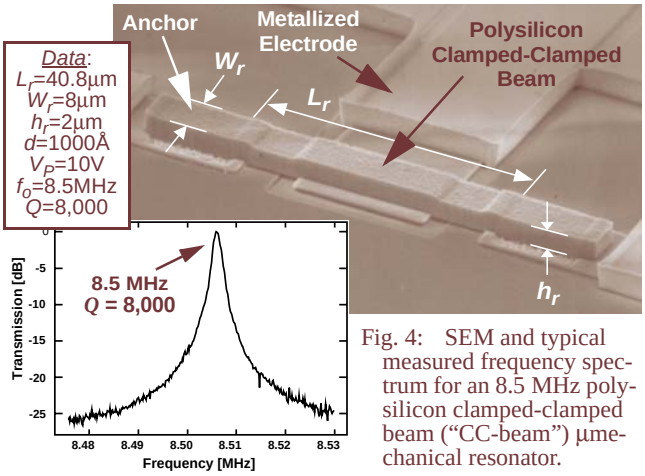

Fig. 4: SEM and typical measured frequency spectrum for an 8.5 MHz polysilicon clamped-clamped beam ("CC-beam") μmechanical resonator.

tures that make them useful as circuit elements: while transistors exhibit high gain, mechanical links exhibit very large Q. By combining the strong points of both circuit elements, on-chip functions previously unachievable are now within the realm of possibilities. We now touch upon a few of these.

B. HF Micromechanical Reference Tank.

The high Q and thermal stability of the resonance frequency of single μmechanical beam elements, such as the 8.5-MHz CC-beam shown in Fig. 4, make them good candidates for tanks in reference oscillator applications. In such applications, the value of the series motional resistance R_x of the resonator is of utmost importance, since it, together with the power handling ability of the resonator, dictates the start-up and noise behavior of a given oscillator. Since $R_x \sim (d^4/V_P^2)$, where d is the electrode-to-resonator gap spacing (c.f., Fig. 2) [4], a wide range of R_x values (e.g., from 10Ω to 10kΩ) can be achieved through proper choice of d and V_P. Often, however, linearity and power supply considerations limit the set of usable R_x values in a given application [7].

C. VHF Micromechanical Reference Tank.

Although impressive at HF, the CC-beam device of Fig. 4 begins to lose a substantial fraction of its internal energy to the substrate at frequencies past 30 MHz, and this limits the attainable Q at VHF. To retain Q's around 8,000 at VHF, a beam with free-free ends is required, such as shown in Fig. 1, in which additional mechanical circuit complexity is added to allow free-free operation, and to reduce anchor losses to the substrate [1]. Via proper support beam design, anchor losses can be greatly attenuated in this structure, and Q's on the order of 8,000 are attained even at 92 MHz.

D. Micromechanical Filters

Among the more useful μmechanical circuits for communications are those implementing low-loss bandpass filters. Figure 5(a) presents the perspective-view schematic of a two-resonator μmechanical filter, comprised of three mechanical links interconnected in a network designed to yield the bandpass spectrum shown in Fig. 5. The design of this filter has been covered extensively in previous literature [5]. For the present purposes, however, the operation of this filter can be deduced from its equivalent circuit, shown in Fig. 5(b). Here, each of the outside links serve as capacitively transduced micromechanical resonators with equivalent circuits as

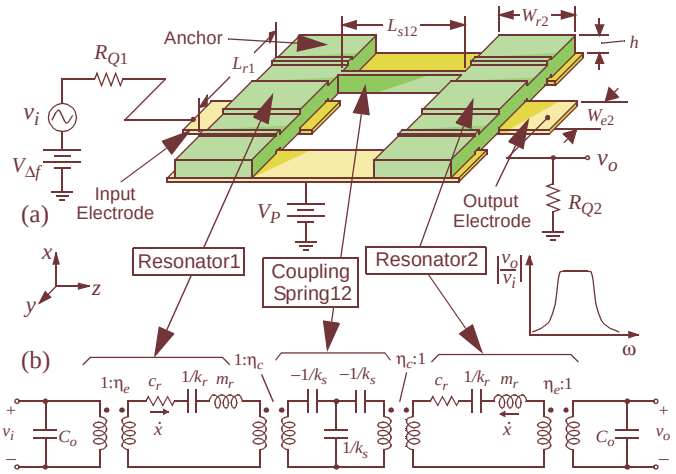

Fig. 5: (a) Schematic of a two-resonator micromechanical filter. (b) Equivalent circuit for the filter of (a) [5].

Table II: Two-Resonator μMechanical Filter Design*

	Gap Spacing, d				
R_Q [Ω] ➠	**300**	**500**	**1,000**	**2,000**	**5,000**
f_o = 70 MHz	195Å	223Å	266Å	317Å	399Å
f_o = 870 MHz	78Å	81Å	80Å	95Å	119Å

* Determined with Q=10,000, BW=1.25MHz, V_P=10V.

shown in Fig. 3. The connecting link actually operates as an acoustic transmission line, and thus, can be modeled by a T-network of energy storage elements.

The filter is excited in a similar fashion to that described in the previous sub-section, with a dc-bias voltage V_P applied to the conductive mechanical network, and an ac signal applied to the input electrode, but this time through an appropriately valued source resistance that loads the Q of the input resonator to flatten the passband [5]. The output resonator of the filter must also see a matched impedance to avoid passband distortion. If the filter is designed symmetrically, with resonator Q's much greater than that of the filter Q_{fltr}, the required value of I/O port termination resistance can be tailored for different applications via the expression

$$R_Q \cong \frac{\sqrt{k_{re} m_{re}}}{q Q_{fltr} \eta_e^2} = \frac{k_{re}}{\omega_o q Q_{fltr} \eta_e^2}, \qquad (4)$$

where e denotes the center location of the electrode, and q is a normalized constant obtainable from filter cookbooks [8]. Of the variables in (4), the electromechanical coupling factor η_e is often the most convenient to adjust for a desired value of termination resistance. Given that $\eta_e \sim (V_P/d^2)$, where d is the electrode-to-resonator gap spacing [5], termination impedance R_Q requirements and bias voltage V_P limitations often dictate the electrode-to-resonator gap spacing for a particular resonator design. This can be seen in Table II.

Figure 6 presents the SEM of a fabricated 7.81-MHz μmechanical filter [5], with a measured frequency characteristic showing less than 1 dB of insertion loss for a 0.22% bandwidth—impressive performance for any passive on-chip filter, made possible by the ultra-high-Q of the constituent

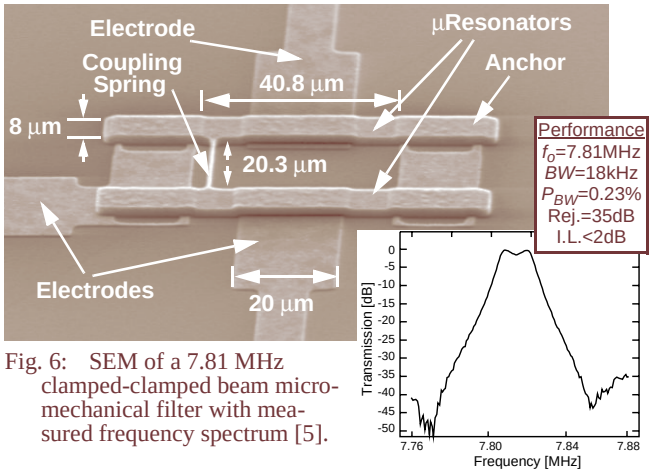

Fig. 6: SEM of a 7.81 MHz clamped-clamped beam micromechanical filter with measured frequency spectrum [5].

μmechanical beam elements.

E. Micromechanical Mixer-Filters

As indicated by (2), the voltage-to-force transducer used by the described resonators is nonlinear, relating input force F_d to input voltage (v_e–v_b) by a square law. When v_b=V_P, this nonlinearity is suppressed, leading to a dominant force that is linear with v_e given by the second term of (3). If, however, signal inputs are applied to both v_e and v_b, a square law mixer results. In particular, if an RF signal v_{RF}=V_{RF}cosω$_{RF}t$ is applied to electrode *e*, and a local oscillator signal v_{LO}=V_{LO}cosω$_{LO}t$ to electrode *b*, then (2) contains the term

$$F_d = \ldots - \frac{1}{2} V_{RF} V_{LO} \frac{\partial C}{\partial x} \cos(\omega_{RF} - \omega_{LO})t + \ldots \qquad (5)$$

which clearly indicates a mixing of *voltage* signals v_{RF} and v_{LO} down to a *force* signal at frequency ω$_{IF}$=(ω$_{RF}$–ω$_{LO}$). If the above transducer is used to couple into a μmechanical filter with a passband centered at ω$_{IF}$, an effective mixer-filter device results that provides both a mixer and filtering function in one passive, micromechanical device.

Figure 7(a) presents the schematic for a symmetrical μmechanical mixer-filter [9], showing the bias and input scheme required for down-conversion and equating this device to a system-level functional block. As shown, since this device provides filtering as part of its function, the overall mechanical structure is exactly that of a μmechanical filter. The only differences are the applied inputs and the use of a non-conductive coupling beam to isolate the IF port from the LO. Note that if the source providing V_P to the second resonator is ideal (with zero source resistance) and the series resistance in the second resonator is small, LO signals feeding across the coupling beam capacitance are shunted to ac ground before reaching the IF port. In reality, finite resistivity in the resonator material allows some amount of LO-to-IF leakage.

The mixer conversion gain/loss in this device is governed primarily by the relative magnitudes of the dc-bias V_P applied to the resonator and the local oscillator amplitude V_{LO}. Using (5), assuming R_Q resistors given by (4), and assuming the filter structure presents a large input impedance to both v_{RF} and v_{LO} (since they are off-resonance), the expression for conversion gain/loss takes the form

$$G_{conv} = \frac{1}{L_{conv}} = \frac{V_{LO}}{V_P} \rightarrow 20\log\left[\frac{V_{LO}}{V_P}\right] \ [\text{dB}]\,. \qquad (6)$$

Note that conversion gain is possible if $V_{LO} > V_P$.

The SSB noise figure for this device derives from a combination of mixer conversion loss, filter insertion loss, and an additional 3dB that accounts for noise conversion from two bands (RF and image) to one, and can be expressed as

$$NF = L_{conv}\big|_{\text{dB}} + L_{fltr}\big|_{\text{dB}} + 3 \quad [\text{dB}]\,, \qquad (7)$$

where $L_{fltr}|_{\text{dB}}$ is the filter insertion loss in dB. Possible values might be $L_{conv}|_{\text{dB}}$=0dB (with V_{LO}=V_P) and $L_{fltr}|_{\text{dB}}$=0.5dB, leading to *NF*=3.5dB—very good calculated performance for a combined mixer and filter using passive components.

III. Receiver RF Front-End Architectures Using MEMS

Having surveyed a subset of the mechanical circuits most useful for communication applications, we now consider methods by which these circuits are best incorporated into communications sub-systems. Three approaches to using micromechanical vibrating resonators are described in order of increasing performance enhancement: (1) direct replacement of off-chip high-*Q* passives; (2) use of an RF channel select architecture using a large number of high-*Q* micromechanical resonators in filter banks and switchable networks; and (3) use of an all-mechanical RF front-end. Since the methods for achieving multi-band reconfigurability using MEMS are obvious, the majority of the discussion in this section will focus on power savings issues.

In proposing these architectures, certain liberties are taken in an attempt to account for potential advances in micromechanical resonator technology. For example, in the RF channel-select architecture, μmechanical circuits are assumed to be able to operate at UHF with *Q*'s on the order of 10,000. Given that TFR's already operate at UHF (but with *Q*'s of

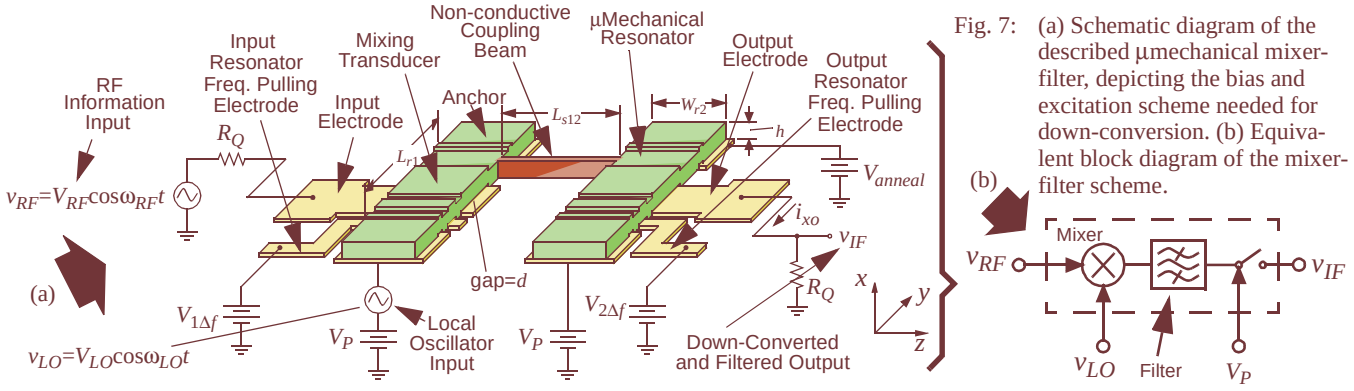

Fig. 7: (a) Schematic diagram of the described μmechanical mixer-filter, depicting the bias and excitation scheme needed for down-conversion. (b) Equivalent block diagram of the mixer-filter scheme.

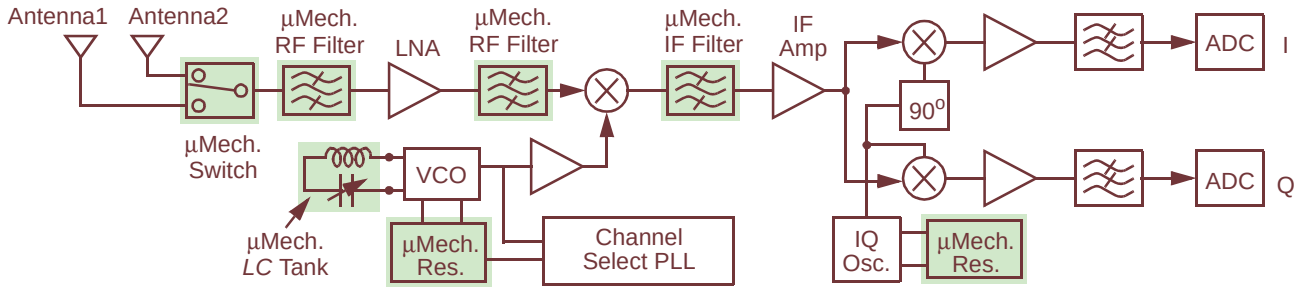

Fig. 8: System block diagram of a super-heterodyne receiver architecture showing potential replacements via MEMS-based components. (On-chip µmechanics are shaded.)

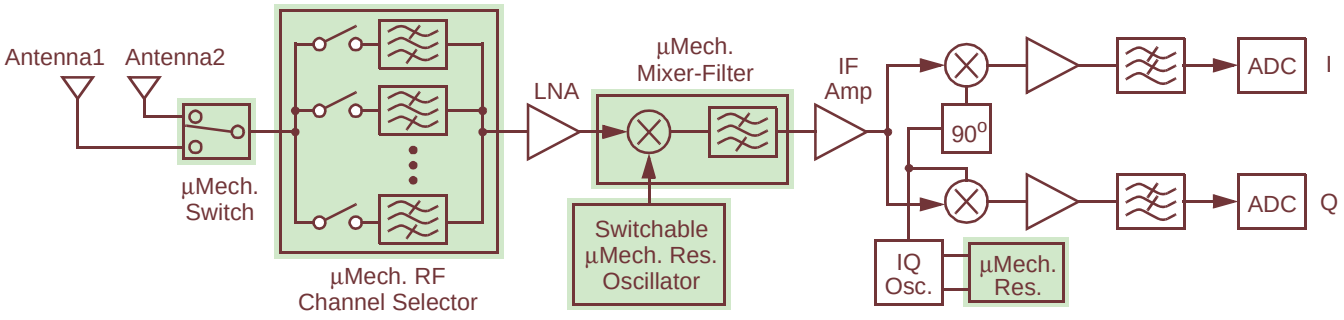

Fig. 9: System block diagram for an RF channel-select receiver architecture utilizing large numbers of micromechanical resonators in banks to trade Q for power consumption. (On-chip µmechanics are shaded.)

1,000), and 100MHz free-free beam µmechanical resonators presently exhibit Q's around 8,000, the above assumed performance values may, in fact, not be far away. At any rate, the rather liberal approach taken in this section is largely beneficial, since it better conveys the potential future impact of MEMS technology, and provides incentive for further advancements in this area. Nevertheless, in order to keep in check the enthusiasm generated here, assumed performances in this section are briefly re-evaluated in the next, with an eye towards practical implementation issues.

A. Direct Replacement of Off-Chip High-Q Passives

Perhaps the most direct way to harness µmechanical circuits is via direct replacement of the off-chip ceramic, SAW, and crystal resonators used in RF pre-select and image-reject filters, IF channel-select filters, and crystal oscillator references. A schematic depicting this approach is shown in Fig. 8. In addition to high-Q components, Fig. 8 also shows the use of other MEMS-based passive components, such as medium-Q micromachined inductors and tunable capacitors [2] used in VCO's and matching networks, as well as low-loss (~0.1dB) µmechanical switches [10] that not only provide enhanced antenna diversity, but that can also yield power savings by making TDD (rather than FDD) more practical in future transceivers.

Of course, the main benefits from the above approach to using MEMS are size reduction and, given the potential for integration of MEMS with transistor circuits, the ability to move more components onto the silicon die. A limited number of performance benefits also result from replacement of existing high-Q passives by µmechanical ones, such as lower overall insertion loss (since µmechanical Q's ~10,000 are larger than those of presently used resonators), and the ability to tailor the termination impedances required by RF and IF filters (c.f., Table II). Such impedance flexibility can be beneficial when designing low-noise amplifiers (LNA's) and mixers in CMOS technology, which presently often consume additional power to impedance match their outputs to 50Ω off-chip components. If higher impedances can be used, for example at the output of an LNA, significant power savings are possible. As an additional benefit, since the source impedance presented to the LNA input is now equal to R_Q, it can now be tailored to minimize noise figure (NF).

Although beneficial, the performance gains afforded by mere direct replacement by MEMS are quite limited when compared to more aggressive uses of MEMS technology. More aggressive architectures will now be described.

B. An RF Channel-Select Architecture

To fully harness the advantages of µmechanical circuits, one must first recognize that due to their micro-scale size and zero dc power consumption, µmechanical circuits offer the same system complexity advantages over off-chip discrete components that planar IC circuits offer over discrete transistor circuits. Thus, to maximize performance gains, µmechanical circuits should be utilized on a massive scale.

Figure 9 presents the system-level block diagram for a possible receiver front-end architecture that takes full advantage of the complexity achievable via µmechanical circuits. The main driving force behind this architecture is power reduction, attained in several of the blocks by trading power for high selectivity (i.e., high-Q). The key power saving blocks in Fig. 9 are now described.

Switchable RF Channel Select Filter Bank.

If channel selection (rather than pre-selection) were possible at RF frequencies (rather than just at IF), then succeeding electronic blocks in the receive path (e.g., LNA, mixer) would no longer need to handle the power of alternate chan-

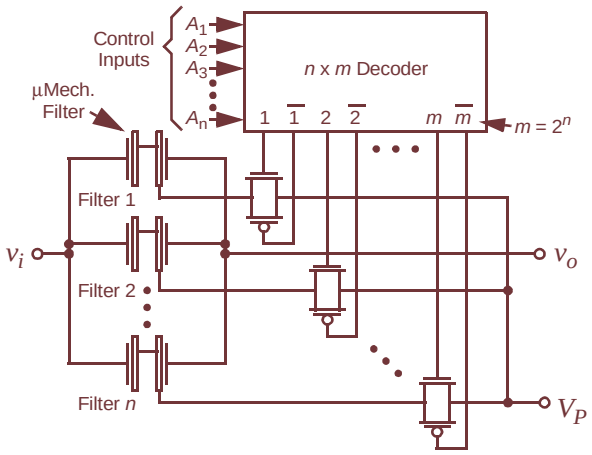

Fig. 10: System/circuit diagram for an RF channel-select micromechanical filter bank.

nel interferers. Thus, their dynamic range can either be greatly relaxed, allowing significant power reductions; or maintained at the same level, in which case a much more robust receiver ensues. In addition, the rejection of adjacent channel interferers also allows reductions in the phase noise requirements of local oscillator (LO) synthesizers, providing further power savings and robustness.

To date, RF channel selection has been difficult to realize via present-day technologies. In particular, low-loss channel selection at RF would require tunable resonators with Q's in the thousands. Unfortunately, however, high-Q often precludes tunability, making RF channel selection via a single RF filter a very difficult prospect.

On the other hand, it is still possible to select individual RF channels via many non-tunable high-Q filters, one for each channel, and each switchable by command. Depending upon the standard, this could entail hundreds or thousands of filters—numbers that would be absurd if off-chip macroscopic filters are used, but that may be perfectly reasonable for micro-scale, passive, µmechanical filters.

Figure 10 presents one fairly simple rendition of the key system block that realizes the desired RF channel selection. As shown, this block consists of a bank of µmechanical filters with all filter inputs connected to a common block input and all outputs to a common block output, and where each filter passband corresponds to a single channel in the standard of interest. In the scheme of Fig. 10, a given filter is switched on (with all others off) by decoder-controlled application of an appropriate dc-bias voltage to the desired filter. (Recall from (2) and (3) that the desired force input and output current are generated in a µmechanical resonator only when a dc-bias V_P is applied; without V_P, there's an open.)

The potential benefits afforded by this RF channel selector can be quantified by assessing its impact on the LNA linearity specification imposed by the IS-98-A interim standard for CDMA cellular mobile stations [11]. In this standard, the required IIP_3 of the LNA is set mainly to avoid desensitization in the presence of a single tone (generated by AMPS [12]) spaced 900kHz away from the CDMA signal center frequency. Here, reciprocal mixing of the local oscillator phase noise with the 900kHz offset single tone and cross-modulation of the single tone with leaked transmitter power outputs dictate that the LNA IIP_3 exceeds +7.6dBm [12]. However, if an RF channel select filter bank such as shown in Fig. 10 precedes the LNA and is able to reject the single tone by 40dB, the requirement on the LNA then relaxes to $IIP_3 \leq -29.3$dBm (assuming the phase noise specification of the LO is *not* also relaxed). Given the well-known noise versus power tradeoffs available in LNA design [13], such a relaxation in IIP_3 can result in nearly an order of magnitude reduction in power. In addition, since RF channel selection relaxes the overall receiver linearity requirements, it may become possible to put more gain in the LNA to suppress noise figure (*NF*) contributions from later stages, while relaxing the required *NF* of the LNA itself, leading to further power savings.

Turning to oscillator power, if the single tone is attenuated to 40dB, then reciprocal mixing with the local oscillator is also greatly attenuated, allowing substantial reduction in the phase noise requirement of the local oscillator. Requirement reductions can easily be such that on-chip solutions to realization of the receive path VCO (e.g., using spiral inductors and pn-diode tunable capacitors) become plausible.

Switchable Micromechanical Resonator Synthesizer.

Although the µmechanical RF channel-selector described above may make possible the use of existing on-chip technologies to realize the receive path VCO, this approach is not recommended, since it denies the system from achieving much greater power reduction factors that may soon be available through MEMS technology. In particular, given that power and Q can often be interchanged when designing for a given oscillator phase noise specification, a better approach to implementing the VCO would be to use µmechanical resonators (with orders of magnitude higher Q than any other on-chip tank) to set the VCO frequency. In fact, with Q's as high as achievable via µmechanics, the basic design methodologies for oscillators must be re-evaluated. For example, in the case where the oscillator and its output buffer contribute phase noise according to Leeson's equation [14], where the $1/f^2$-to-white phase noise corner occurs at $(f_o/(2Q))$, a tank Q>1,500 is all that would be required to move the $1/f^2$-to-white phase noise corner close enough to the carrier that only white phase noise need be considered for CDMA cellular applications, where the phase noise power at frequency offsets from 285kHz to 1515kHz is most important. If only white noise is important, then only the output buffer noise need be minimized, and sustaining amplifier noise may not even be an issue. If so, the power requirement in the sustaining amplifier might be dictated solely by loop gain needs (rather than by phase noise needs), which for a µmechanical resonator-based VCO with R_x~40Ω, L_x~84µH, and C_x~0.5fF, might be less than 1mW.

To implement a tunable local oscillator synthesizer, a switchable bank is needed, similar to that of Fig. 10 but using µmechanical resonators, not filters, each corresponding to one of the needed LO frequencies, and each switchable into or out of the oscillator sustaining circuit [4]. Note that because µmechanical resonators are now used in this implementation, the Q and thermal stability (with compensation) of the oscillator may now be sufficient to operate without the need for locking to a lower frequency crystal reference. The

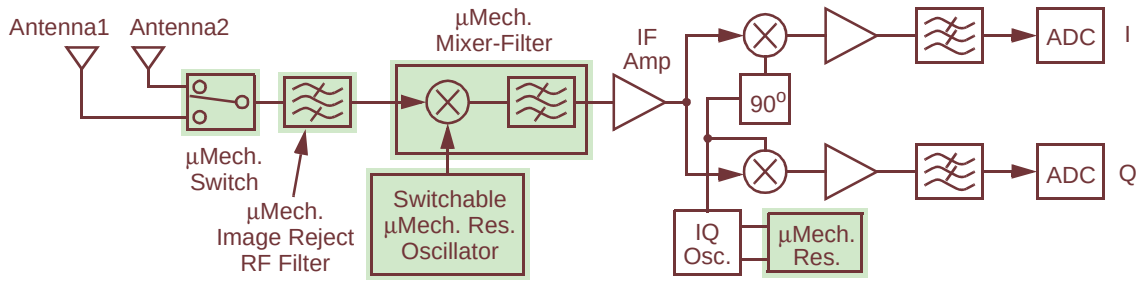

Fig. 11: System-block diagram for an all-MEMS RF front-end receiver architecture. (On-chip µmechanics are shaded.)

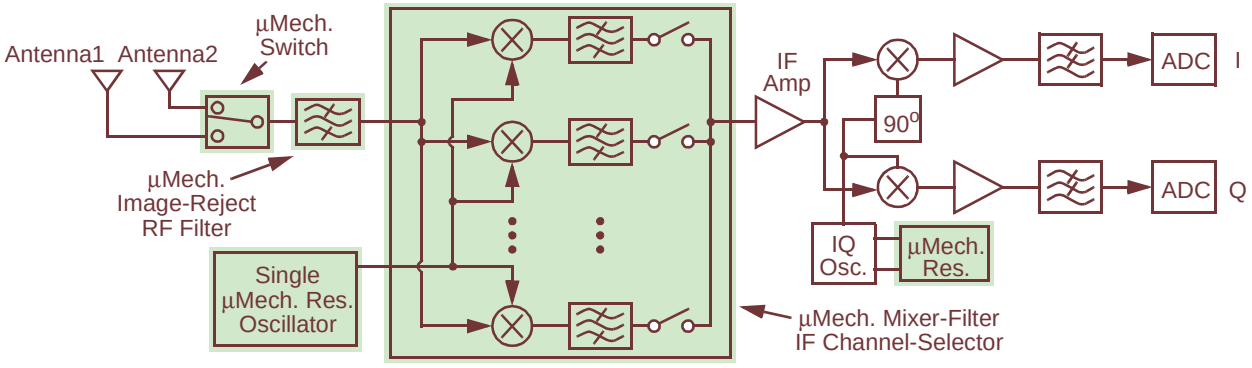

Fig. 12: System block diagram for an all-MEMS receiver front-end, employing an RF image-reject filter, a fixed µmechanical resonator local oscillator, and a switchable array of IF µmechanical mixer-filters. (On-chip µmechanics are shaded.)

power savings attained upon removing the PLL and prescaler electronics needed in past synthesizers can obviously be quite substantial. In effect, by implementing the synthesizer using µmechanical resonators, synthesizer power consumption can be reduced from the ~90mW dissipated by present-day implementations using medium-Q L and C components [15], to something in the range of only 1-4 mW. Again, all this is attained using a circuit topology that would seem absurd if only macroscopic high-Q resonators were available, but that becomes plausible in the µmechanical arena.

Micromechanical Mixer-Filter.

The use of a µmechanical mixer-filter in the receive path of Fig. 9 eliminates the dc power consumption associated with the active mixer normally used in present-day receiver architectures. This corresponds to a power savings on the order of 10-20 mW. In addition, if a multiple input electrodes (one for RF, one for matching) are used for the mixer-filter, the RF input can be made to appear purely capacitive to the LNA (i.e., at the RF frequency), and the LNA would no longer require a driver stage to match a certain impedance. Rather, an inductive load can be used to resonate the capacitance, as in [13], allowing power savings similar to that discussed in Section III.A.

C. An All-MEMS RF Front-End Receiver Architecture

In discussing the above MEMS-based architecture, one very valid question may have arisen: If µmechanical filters and mixer-filters can truly post insertion losses consistent with their high-Q characteristics, then is an LNA really required at RF frequencies? It is this question that inspires the receiver architecture shown in Fig. 11, which depicts a receive path comprised of a relatively wideband image reject µmechanical RF filter followed immediately by a narrowband IF mixer-filter that then feeds subsequent IF electronics. The only active electronics operating at RF in this system are those associated with the LO, which if it uses a bank of µmechanical resonators, can operate at 1-4 mW. If plausible, the architecture of Fig. 11 clearly presents enormous power advantages, eliminating completely the power consumption of the LNA and active mixer of Fig. 8—a total power savings on the order of 40mW—and, together with the µmechanical LO, substantially increasing mobile phone standby times.

To assess the plausibility of this all-MEMS front-end, one can determine whether or not this scheme yields a reasonable noise figure requirement at the input node of the IF amplifier in Fig. 11. An expected value for RF image reject filter insertion loss is IL~0.2dB, assuming that three resonators are used, each with Q=5,000. Using the value for mixer-filter NF_{mf}=3.5dB projected in Section II, the total combined NF_{f+mf}=3.7dB. Given IS-98-A's requirement that the receiver NF_{RX}≤7.8dB, the needed value at the IF amplifier input is NF_{IF}≤4.1dB, which can be reasonable if the IF amplifier gain can be increased to suppress the noise of succeeding stages.

It should be noted that Fig. 11 represents only one of many possible all-MEMS front-end topologies. For example, instead of using a MEMS array in the high-frequency local oscillator synthesizer as done in Fig. 11, the array complexity can be moved to lower frequencies, such as done in Fig. 12, where the LO is now a fixed oscillator using only one UHF µmechanical resonator tank, and where a switchable array of mixer-filter devices is now employed to do IF channel-selection. Although it entails greater mechanical circuit complexity since many mixer-filter circuits are now needed (instead of many single resonators), the architecture of Fig. 12 might actually be preferred over that of Fig. 11, since its µmechanical array is now only at the much lower IF frequency, rather than at RF.

Although the all-MEMS front-end architectures of

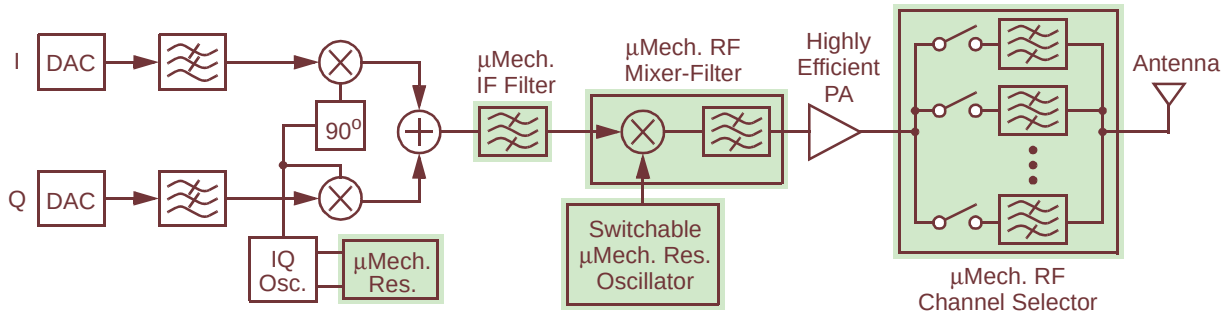

Fig. 13: RF channel-select transmitter architecture, possible only if high power µmechanical resonators can be achieved. Here, on-chip µmechanical blocks are shaded, and the PA is not necessarily implemented on-chip.

Figs. 11 and 12 may at first seem the most preposterous of the bunch, early versions of the primary filtering and mixing devices required for their implementation have already been demonstrated. In particular, TFR image-reject filters have been demonstrated at UHF frequencies with insertion losses of less than 3dB [6]. It should be noted, however, that the first demonstrated mixer-filter based on polysilicon clamped-clamped beam µmechanical resonators achieved NF_{mf}=15dB [9]—quite worse than the 3.5dB used in the above calculation, and in fact, a value that precludes the use of Figs. 11 or 12. It is not unreasonable, however, to expect that future renditions of mixer-filters, perhaps using more appropriate resonators (e.g., higher *Q* free-free beams, rather than clamped-clamped), might be able to achieve the projected 3.5dB.

IV. An RF Transmitter Architecture Using MEMS

Due to a lack of sufficient in-band power handling capability, very little consideration has been given to date to the possibility of using µmechanical resonators in the transmit path. However, research efforts are presently underway to remedy this, and if successful, equally compelling MEMS-based transmit architectures can also be proposed.

Figure 13 depicts one rendition, in which an RF channel-selector is placed after the power amplifier (PA) in the transmit path. This channel selector might utilize a similar circuit as that of Fig. 10, but using µmechanical resonators with sufficient power handling capability. Assuming for now that such devices are possible, this transmit topology could provide enormous power savings. In particular, if a high-*Q*, high-power filter with less than 1dB of insertion loss could follow the PA, cleaning all spurious outputs, including those arising from spectral regrowth, then more efficient PA designs can be utilized, despite their nonlinearity. For example, a PA previously restricted by linearity considerations to 30% efficiency in present-day transmitter architectures, may now be operable closer to its maximum efficiency, perhaps 50%. For a typical transmit power of 600mW, this efficiency increase corresponds to 800mW of power savings. If a more efficient PA topology could be used, such as Class E, with theoretical efficiencies approaching 100%, the power savings could be much larger.

In addition to the MEMS-based channel-select RF filter bank, the architecture of Fig. 13 also features a micromechanical up-converter that uses a mixer-filter device, such as described in Section II.E, to up-convert and filter the information signal before directing it to the power amplifier.

V. Research Issues

As stated at the beginning of Section III, the transceiver architectures described above rely to some extent on performance characteristics not yet attained by µmechanical resonators, but targeted by ongoing research efforts. Specifically, µmechanical devices with the following attributes have been assumed: (1) adequate *Q* at UHF frequencies; (2) sufficient linearity and power handling capability; (3) usable port impedances; and (4) massive scale integration methods.

A. Frequency and Q

Table I of Section II showed that from a purely geometric perspective, the frequencies required by the architectures of Section III are reasonable. However, frequency is not really the main issue; *Q* is. The most important question is whether high-*Q* can be maintained as frequencies increase, since new loss mechanisms may be introduced as frequencies increase. As an already mentioned case in point, anchor losses in clamped-clamped beams become excessive past 50MHz, making free-free beams (that effectively remove anchors) much more suitable for mid-VHF and UHF frequencies [1]. What loss mechanisms await at GHz frequencies for flexural-mode resonators is, as yet, unknown. However, as mentioned in Section II, *Q*'s of over 1,000 at UHF (and beyond) have already been achieved via 200 µm-diameter thin-film bulk acoustic resonators (FBAR's) based on longitudinal resonance modes and piezoelectric structural materials [6]. Although not the *Q* of 10,000 needed for RF channel-select applications, the *Q*'s attained by FBAR's at GHz frequencies constitute a proof of concept for vibrating mechanical resonators, and with the availability of better structural materials (e.g., LPCVD polysilicon, instead of sputtered AlN), it is not implausible that µmechanical resonators may yet achieve *Q* ~10,000 at GHz frequencies.

Still, there are concerns that "scaling-induced" performance limitations, such as adsorption-desorption noise [16], thermal fluctuation noise [16], power handling limitations [7], and *Q* loss due to increases in surface-to-volume ratio as devices are scaled [17], will ultimately limit the frequency range of µmechanical resonators. To suppress such "scaling-induced" limitations, more recent µmechanical resonator designs now use extensional, rather than flexural vibration modes, to allow UHF frequencies while avoiding sub-µm dimensions. The 34 µm-diameter radial contour-mode disk resonator shown in Fig. 14 is one such device, which vibrates via uniform, well-balanced, radial expansion and contraction

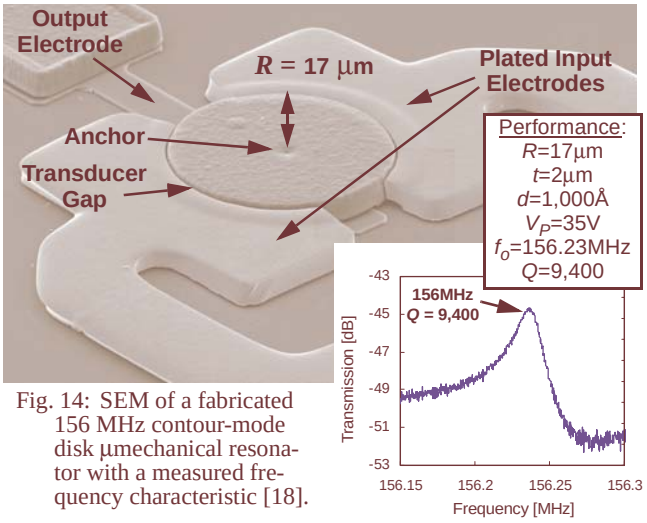

Fig. 14: SEM of a fabricated 156 MHz contour-mode disk μmechanical resonator with a measured frequency characteristic [18].

along its perimeter to achieve a Q >9,000 at 156 MHz [18]. It is not unreasonable to expect this device to maintain similar Q values when scaled beyond 1 GHz.

B. Linearity and Power Handling

Macroscopic high-Q filters based on ceramic resonator or SAW technologies are very linear in comparison with the transistor blocks they interface with in present-day transceivers. As a result, their contributions the total IIP_3 budget can generally be ignored in the majority of designs. Although capacitively transduced μmechanical resonators are generally more linear than transistor circuits, with semi-empirical IIP_3's of +12dB for 2μm-thick 70MHz resonators [5], they are still much less linear than their off-chip macroscopic counterparts. The degree to which this impacts the utility of the architectures proposed in Section III depends upon the standard being implemented. For example, an IIP_3 of +12dB is sufficient for most receive applications, except for those in standards that allow simultaneous transmit and receive (such as CDMA), where the RF pre-select filter is required to reject out-of-band transmitter outputs to alleviate cross-modulation phenomena [12]. For such situations, at least at present, a more linear filter must precede the filter bank of Fig. 10 if cross-modulation is to be sufficiently suppressed. This additional filter, however, can now have a very wide bandwidth, as it has no other purpose than to reject transmitter outputs. Thus, it may be realizable with very little insertion loss using on-chip (μmachined) inductor and capacitor technologies [2].

Still, μmechanical circuits with high power handling capability would not only present a better solution to the above, but might also enable the very aggressive transmit architecture of Fig. 13. To this end, alternative geometries (e.g., no longer flexural mode) and the use of alternative transduction methods (e.g., piezoelectric, magnetostrictive) are presently under study. Techniques for combining devices to increase power capacity are also being explored.

C. Resonator Impedance

Thin-film bulk acoustic resonators can already impedance match to conventional antennas, so if their frequency, Q, yield, size, and integration capacity are adequate for a given architecture (e.g., the all-MEMS architectures of Section III), then they present a very good solution. If higher Q is needed, however, then μmechanical resonators may be better suited for the given application. From Table II, RF μmechanical filters should be able to match to 300Ω impedances, provided their electrode-to-resonator gaps can be made down to d~80Å. Since electrode-to-resonator gaps are achieved via a process very similar to that used to achieve MOS gate oxides [5], such gaps are not unreasonable. However, device linearity generally degrades with decreasing d, so practical designs must balance linearity with impedance requirements [5].

In cases where linearity issues constrain the minimum d to a value larger than that needed for impedance matching (assuming a fixed V_P), several μmechanical filters with identical frequency characteristics may be used to divide down the needed value of termination impedance. For example, ten of the filters in the fourth column of Table II can be hooked up in parallel to realize an R_Q=2000/10=200Ω. Note that the use of numerous filters in parallel also increases the power handling threshold. For example, if a given micromechanical filter were designed to handle 10 mW of power while retaining adequate linearity, then ten of them will handle 100 mW.

Once again, the ability to use of numerous high-Q elements in complex micromechanical circuits without regard to size greatly extends the applicable range of micromechanical signal processors. Given a suitable massive-scale trimming technique, the above parallel filter solution may work well even in the transmit path, perhaps making plausible power saving transmit architectures, such as that of Fig. 13.

D. Fabrication Technologies

To date, surface μmachining technologies have been used quite successfully to realize fully integrated circuit-MEMS products in high volume, and in some cases, at LSI complexities [19,20]. In addition, adaptive circuit-MEMS technologies are now emerging that separate the circuits and MEMS processes into modules, allowing integration of virtually any circuit process with a given MEMS technology. A variety of modular integration approaches have recently been demonstrated, including fully planar processes where the MEMS module is done either before [21] or after (c.f., Fig. 15 [22,23]) the circuits module, as well as techniques based upon wafer-level bonding [24,25] (perhaps the ultimate in modularity). Meanwhile, on-chip vacuum encapsulation processes (needed for high-Q and environmental protection) are also receiving focused attention, with many approaches now under study, including ones based upon bonding technologies [26], and others based upon planar processing where three or four additional masking steps are utilized to form sealable caps over microstructures [27]. Finally, frequency trimming methods are also a subject of ongoing research [28].

VI. Conclusions

Vibrating μmechanical resonators constitute the building blocks for a new integrated mechanical circuit technology in which high Q serves as a principal design parameter that enables more complex circuits. By combining the strengths of integrated μmechanical and transistor circuits, using both in massive quantities, previously unachievable functions become possible that enable transceiver architectures with projections for orders of magnitude performance gains. In particular, with the addition of high-Q μmechanical circuits,

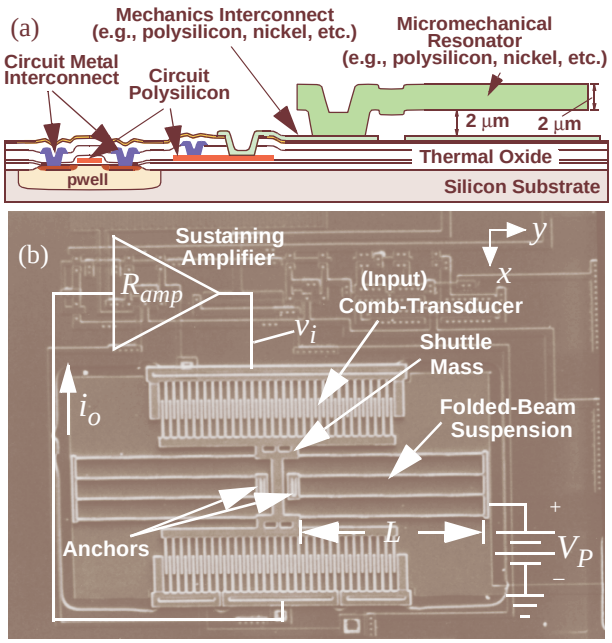

Fig. 15: (a) Cross-section of the MICS process [22]. (b) Overhead-view of a fully integrated micromechanical resonator oscillator fabricated using MICS [22].

paradigm-shifting transceiver architectures that trade power for selectivity (i.e., *Q*) become possible, with the potential for substantial power savings and multi-band reconfigurability. To reap the benefits of these new architectures, however, further advancements in device frequency, linearity, and manufacturability are required. Research efforts are ongoing.

Acknowledgment: The majority of this work was supported under grants from DARPA and NSF.

References

[1] K. Wang, A.-C. Wong, and C. T.-C. Nguyen, "VHF free-free beam high-*Q* micromechanical resonators," *IEEE/ASME J. Microelectromech. Syst.*, vol. 9, no. 3, pp. 347-360, Sept. 2000.

[2] C. T.-C. Nguyen, L. P.B. Katehi, and G. M. Rebeiz, "Micromachined devices for wireless communications (invited)," *Proc. IEEE*, vol. 86, no. 8, pp. 1756-1768, Aug. 1998.

[3] J. M. Bustillo, R. T. Howe, and R. S. Muller, "Surface micromachining for microelectromechanical systems," *Proc. IEEE*, vol. 86, no. 8, pp. 1552-1574, Aug. 1998.

[4] C. T.-C. Nguyen, "Micromechanical circuits for communication transceivers (invited)," *Proceedings*, 2000 Bipolar/BiCMOS Circuits and Technology Meeting (BCTM), Minneapolis, Minnesota, September 25-26, 2000, pp. 142-149.

[5] F. D. Bannon III, J. R. Clark, and C. T.-C. Nguyen, "High frequency micromechanical filters," *IEEE J. Solid-State Circuits*, vol. 35, no. 4, pp. 512-526, April 2000.

[6] K. M. Lakin, G. R. Kline, and K. T. McCarron, "Dev. of miniature filters for wireless applications," *IEEE Trans. Microwave Theory Tech.*, vol. 43, no. 12, pp. 2933-2939, Dec. 1995.

[7] R. Navid, J. R. Clark, M. Demirci, and C. T.-C. Nguyen, "Third-order intermodulation distortion in capacitively-driven CC-beam micromechanical resonators," *Tech. Digest*, 14th Int. IEEE Micro Electro Mechanical Systems Conf., Interlaken, Switzerland, Jan. 21-25, 2001, pp. 228-231.

[8] A. I. Zverev, *Handbook of Filter Synthesis*, New York: John Wiley & Sons, 1967.

[9] A.-C. Wong, H. Ding, and C. T.-C. Nguyen, "Micromechanical mixer+filters," *Tech. Dig.*, IEEE Int. Electron Devices Meeting, San Francisco, CA, Dec. 6-9, 1998, pp. 471-474.

[10] Z. Jamie Yao, S. Chen, S. Eshelman, D. Denniston, and C. Goldsmith, "Micromachined low-loss microwave switches," *J. Microelectromech. Syst.*, vol. 8, no. 2, pp. 129-134, June 1999.

[11] "Recommended minimum performance standards for dual-mode wideband spread spectrum cellular mobile stations," *TIA/EIA/IS-98-A Interim Standard*, July 1996.

[12] W. Y. Ali-Ahmad, "RF system issues related to CDMA receiver specifications," *RF Design*, pp. 22-32, Sept. 1999.

[13] D. K. Shaeffer and T. H. Lee, "A 1.5-V, 1.5-GHz CMOS low noise amplifier," *IEEE J. Solid-State Circuits*, vol. 32, No. 5, pp. 745-759, May 1997.

[14] D. B. Leeson, "A simple model of feedback oscillator noise spectrum," *Proc. IEEE*, vol. 54, pp. 329-330, Feb. 1966.

[15] J. F. Parker and D. Ray, "A 1.6-GHz CMOS PLL with on-chip loop filter," *IEEE J. Solid-State Circuits*, vol. 33, no. 3, pp. 337-343, March 1998.

[16] J. R. Vig and Y. Kim, "Noise in microelectromechanical system resonators," *IEEE Trans. Utrason. Ferroelec. Freq. Contr.*, vol. 46, no. 6, pp. 1558-1565, Nov. 1999.

[17] K. Y. Yasumura, T. D. Stowe, E. M. Chow, T. Pfafman, T. W. Kenny, B. C. Stipe, and D. Rugar, "Quality factors in micron- and submicron-thick cantilevers," *IEEE/ASME J. Microelectromech. Syst.*, vol. 9, no. 1, pp. 117-125, March 2000.

[18] J. R. Clark, W.-T. Hsu, and C. T.-C. Nguyen, "High-*Q* VHF micromechanical contour-mode disk resonators," *Tech. Digest*, IEEE Int. Electron Devices Meeting, San Francisco, California, Dec. 11-13, 2000, pp. 399-402.

[19] T. A. Core, W. K. Tsang, S. J. Sherman, "Fabrication technology for an integrated surface-micromachined sensor," *Solid State Technology*, pp. 39-47, Oct. 1993.

[20] L. J. Hornbeck, T. R. Howell, R. L. Knipe, and M. A. Mignardi, "Digital micromirror device—commercialization of a massively parallel MEMS technology," *Microelectronic Systems 1997*, DSC-Vol. 62, ASME International Mechanical Engineering Congress and Exposition (1997), pp. 3-8.

[21] J. H. Smith, S. Montague, J. J. Sniegowski, J. R. Murray, *et al.*, "Embedded micromechanical devices for the monolithic integration of MEMS with CMOS," *Tech. Dig.*, IEEE Int. Electron Devices Mtg, Wash., D.C., Dec. 10-13, 1995, pp. 609-612.

[22] C. T.-C. Nguyen and R. T. Howe, "An integrated CMOS micromechanical resonator high-*Q* oscillator," *IEEE J. Solid-State Circuits*, vol. 34, no. 4, pp. 440-455, April 1999.

[23] A. E. Franke, D. Bilic, D. T. Chang, P. T. Jones, T.-J. King, R. T. Howe, and G. C. Johnson, "Post-CMOS integration of germanium microstructures," *Tech. Digest*, 12th Int. IEEE MEMS Conf., Orlando, Florida, Jan. 17-21, 1999, pp. 630-637.

[24] A. Singh, D. A. Horsley, M. B. Cohn, A. P. Pisano, and R. T. Howe, "Batch transfer of microstructures using flip-chip solder bonding," *J. Microelectromech. Syst.*, vol. 8, no. 1, pp. 27-33, March 1999.

[25] A.-C. Wong, Y. Xie, and C. T.-C. Nguyen, "A bonded-microplatform technology for modular merging of RF MEMS and transistor circuits," *Tech. Dig.*, the 11th Int. Conf. on Solid-State Sensors & Actuators (Transducers'01), Munich, Germany, June 10-14, 2001, pp. 992-995.

[26] Y.-T. Cheng, W.-T. Hsu, L. Lin, C. T.-C. Nguyen, and K. Najafi, "Vacuum packaging using localized aluminum/silicon-to-glass bonding," *Tech. Dig.*, 14th Int. IEEE Micro Electro Mechanical Systems Conf., Interlaken, Switzerland, Jan. 21-25, 2001, pp. 18-21.

[27] K. S. Lebouitz, A. Mazaheri, R. T. Howe, and A. P. Pisano, "Vacuum encapsulation of resonant devices using permeable polysilicon," *Technical Digest*, 12th Int. IEEE MEMS Conf., Orlando, Florida, Jan. 17-21, 1999, pp. 470-475.

[28] K. Wang, A.-C. Wong, W.-T. Hsu, and C. T.-C. Nguyen, "Frequency-trimming and *Q*-factor enhancement of micromechanical resonators via localized filament annealing," *Tech. Dig.*, Transducers'97, Chicago, IL, June 16-19, 1997, pp. 109-112.